NASA TECHNICAL NOTE

NASA TN D-5252

c.1

NASA TN D-5252

A TECHNIQUE TO INFER ATMOSPHERIC WATER-VAPOR MIXING RATIO FROM MEASURED HORIZON RADIANCE PROFILES

by Thomas B. McKee, Ruth I. Whitman, and Jules J. Lambiotte, Jr.

Langley Research Center
Langley Station, Hampton, Va.

NATIONAL AERONAUTICS AND SPACE ADMINISTRATION • WASHINGTON, D. C. • JUNE 1969

A TECHNIQUE TO INFER ATMOSPHERIC WATER-VAPOR MIXING RATIO FROM MEASURED HORIZON RADIANCE PROFILES

By Thomas B. McKee, Ruth I. Whitman,
and Jules J. Lambiotte, Jr.

Langley Research Center
Langley Station, Hampton, Va.

NATIONAL AERONAUTICS AND SPACE ADMINISTRATION

For sale by the Clearinghouse for Federal Scientific and Technical Information
Springfield, Virginia 22151 – CFSTI price $3.00

A TECHNIQUE TO INFER ATMOSPHERIC WATER-VAPOR MIXING RATIO FROM MEASURED HORIZON RADIANCE PROFILES

By Thomas B. McKee, Ruth I. Whitman,
and Jules J. Lambiotte, Jr.
Langley Research Center

SUMMARY

A technique is presented to infer atmospheric water-vapor mixing-ratio structure from measured horizon radiance profiles when a method exists for calculating radiance profiles. The technique was implemented for the spectral interval, 315 cm^{-1} to 475 cm^{-1}, of the rotational water-vapor band but the technique is not limited to that interval. Inferred mixing-ratio accuracy for the 10-km to 35-km altitude range is shown when the computer program input data contain no errors and when the computer program input is perturbed by errors normally found in measurements. Water-vapor mixing ratios have been inferred from horizon radiance profiles measured in the summer in a latitude range from 17° North to 58° North from an NASA Project Scanner flight. No significant latitudinal variation existed above an altitude of 18 km. Below 18 km a latitudinal variation does exist that is consistent with the large variations that are known to exist in the troposphere. The mixing ratio decreases with altitude to a minimum at a point ranging from 3 km to 5 km above the tropopause altitude. Above an altitude of 20 km the mixing ratio shows a slight increase to 35 km.

INTRODUCTION

The objective of NASA's Project Scanner was to measure horizon radiance profiles of the earth which would provide a better understanding of the primary input to horizon sensing devices. Horizon radiance profiles were measured in two spectral bands of the strongly absorbing atmospheric constituents: 615 cm^{-1} to 715 cm^{-1} of the carbon dioxide (CO_2) molecule and 315 cm^{-1} to 475 cm^{-1} of the water-vapor (H_2O) molecule. A description of the project and the results for summer measurements are given in reference 1. Results for winter measurements are presented in reference 2. An attempt was made to estimate the temperature and pressure structure of the atmosphere in the geographic regions where measurements were taken so that radiance profiles could be independently predicted. Unfortunately, the water-vapor mixing ratio is not routinely measured to altitudes that are sufficiently high to be useful in calculating horizon radiance profiles.

A natural outgrowth of the effort to predict radiance profiles analytically was to reverse the problem and use measured horizon radiance profiles to infer water-vapor mixing ratio in the atmosphere. The favorable geometry which characterizes tangential viewing has been used previously to allow inference of atmospheric temperature. (See ref. 3.) A thorough review of measurements of water-vapor mixing ratio in the upper troposphere and lower stratosphere at balloon altitudes is given in reference 4. Most of the measurements have been made with frost-point hygrometers; however, other methods have been employed which used either absorption spectroscopy with the sun as a source or emission by water vapor in the 6.5μ band. (See ref. 5.) Inference of water-vapor mixing ratio from the measurement of water-vapor emission as a function of frequency viewing in the nadir has been described in references 6 and 7.

This report describes a technique which allows the inference of water-vapor mixing ratio structure from a measured horizon radiance profile. A very limited number of mixing ratios inferred with this technique has been given in references 1 and 2. The derivation and application of the technique are presented for the 315 cm^{-1} to 475 cm^{-1} spectral interval of the H_2O molecule but are not limited to that interval. Sensitivity of the method to various errors is examined for this spectral interval. The method is applied to the summer data of reference 1 to show the mixing-ratio structure over a wide latitude range.

SYMBOLS

C_1	constant, 1.1909×10^{-5} erg-centimeter^2/second-steradian
C_2	constant, 1.4389 centimeters-degrees
c	proportionality constant, centimeter^{-1}
G	integral ratio, dimensionless
GMT	Greenwich mean time
H	tangent height, kilometers
h	altitude, kilometers
J_ν	source function, watts/meter^2-steradian-centimeter^{-1}

N	radiance, watts/meter^2-steradian
N_c	calculated radiance, watts/meter^2-steradian
N_m	measured radiance, watts/meter^2-steradian
N_ν	spectral radiance, watts/meter^2-steradian-centimeter^{-1}
s	distance along line of sight, kilometers
T	temperature, degrees Kelvin
w	water-vapor mixing ratio, ratio of density of water vapor to density of dry air, grams/kilogram
ν	wave number, centimeter^{-1}
τ	transmittance, dimensionless

Subscripts:

l	lower limit of integration
u	upper limit of integration
o	values at outer boundary of iteration technique
1,2,3,4	points along line of sight

A prime denotes values used in iteration process.

DERIVATION OF TECHNIQUE

The technique employed to infer atmospheric water-vapor content is an iterative process applied to the equation of radiative transfer used to calculate horizon radiance profiles. This section contains a discussion of the calculation of radiance profiles and then the derivation of the inferred water-vapor mixing ratio.

Calculation of Radiance Profiles

An instrument (observer) with a small field of view was positioned outside the atmosphere to measure horizon radiance profiles as it scanned across the horizon (limb). One line of sight through the atmosphere is shown in figure 1.

The tangent height was used to position the line of sight with respect to the surface of the earth. The tangent height is defined as the distance along the radius vector from the surface of the earth to a point where the radius vector is normal to the line of sight. A radiance profile $N(H)$ is then radiance as a function of tangent height.

The radiance exiting the atmosphere along a line of sight is given by the equation of radiative transfer (see ref. 8):

$$N(H) = -\int_{\nu}\int_{s} J_{\nu}\frac{\partial\tau}{\partial s}\,ds\,d\nu + \int_{\nu} J_{\nu}\tau_1\,d\nu \tag{1}$$

Any calculation of a radiance profile must evaluate equation (1) at different tangent heights. When the second or boundary term in equation (1) is ignored, the radiance from a lower boundary, that is, clouds or the earth's surface, cannot be considered. In the rotational water-vapor band clouds do affect the radiance profiles significantly, but the decision was made to ignore the boundary term to facilitate the computations. This decision is not as restrictive as it may appear at first. When the line of sight does not intercept a cloud, the boundary term is not needed; therefore, for all clear atmospheres and for all tangent heights above the clouds the calculation is complete. In figure 1 the transmittance τ_1 is either to the boundary or to the edge of the atmosphere. For the present problem let the source function be restricted to thermal radiation from gasses in the atmosphere; then the source function can be expressed as the ideal Planck radiation where

$$J_{\nu} = N_{\nu} = \frac{C_1\nu^3}{\exp\left(\frac{C_2\nu}{T}\right) - 1} \tag{2}$$

By substituting equation (2) into equation (1) and ignoring the second or boundary term, equation (1) becomes

$$N(H) = -\int_{\nu}\int_{s} N_{\nu}\frac{\partial\tau}{\partial s}\,ds\,d\nu \tag{3}$$

Usually, equation (3) is transformed into an integration over transmittance and wave number and is evaluated as

$$N(H) = -\int_{\nu} \int_{\tau} N_{\nu} \, d\tau \, d\nu \tag{4}$$

Since the Project Scanner measured data are for the 315 cm^{-1} to 475 cm^{-1} spectral interval of an absorption band of the H_2O molecule, the rest of this report will be in terms of the 315 cm^{-1} to 475 cm^{-1} spectral band. The technique, however, is applicable to other spectral bands. For the present work, the evaluation of equation (1) is described in detail in reference 9. Transmittance data used were from reference 10. To calculate the radiance profile $N(H)$ in the 315 cm^{-1} to 475 cm^{-1} interval from equation (4), the atmospheric parameters, temperature, pressure, and mixing ratio of H_2O as a function of altitude are required. The Planck function (spectral radiance) N_{ν} is dependent only on temperature, whereas the transmittance is dependent on geometry, temperature, pressure, and the mixing ratio of H_2O.

To determine whether an iterative technique to obtain the mixing ratio of water is attractive, equation (4) can be rewritten into the sum of three integrals along the line of sight:

$$N(H) = -\int_{\nu_u}^{\nu_l} \int_{1}^{\tau_3} N_{\nu} \, d\tau \, d\nu - \int_{\nu_u}^{\nu_l} \int_{\tau_3}^{\tau_2} N_{\nu} \, d\tau \, d\nu - \int_{\nu_u}^{\nu_l} \int_{\tau_2}^{\tau_1} N_{\nu} \, d\tau \, d\nu \tag{5}$$

When the atmosphere is spherically stratified (as shown in fig. 1), the geometric length along the line of sight is much greater for the first layer above the tangent point than for any other layer. In addition to the geometric factor, the density decreases with altitude and further emphasizes that most of the atmospheric mass along the line of sight is near the tangent point.

The fractional radiance contribution to equation (5) from the region τ_3 to τ_2 is given by

$$G(H) = \frac{-\int_{\nu} \int_{\tau_3}^{\tau_2} N_{\nu} \, d\tau \, d\nu}{N(H)} \tag{6}$$

Figure 2 shows $G(H)$ for a 1-km-thick layer as a function of H for the spectral interval 315 cm^{-1} to 475 cm^{-1} calculated by using the 1962 U.S. Standard Atmosphere (table I) and the reference mixing ratio (table II). For tangent heights from 9 km to 32 km, the layer above the tangent point contributes 39 to 46 percent of the radiance. As long as the second integral in equation (5) provides a workable portion of the radiance along the line of sight, it appears that the second integral in equation (5) could have a sufficient amount of new information each time the mixing ratio is changed to make an iterative technique

attractive. Figure 2 indicates that the significance of the central layer reduces rapidly below a tangent height H of 9 km; for instance, the central layer contributes only 3 percent of the radiance at a tangent height H of 5 km. As the contribution of the second integral in equation (5) is reduced, it is to be expected that the lower boundary of an iteration technique using the second term of equation (5) would be reached where convergence would be slow and where errors could be magnified.

Derivation of Inferred Water-Vapor Mixing Ratio

In order to infer water-vapor mixing ratio from measured horizon radiance profiles, four assumptions are required:

(1) A transmittance model

(2) Temperature as a function of altitude

(3) Pressure as a function of altitude

(4) Absence of clouds

These assumptions are necessary since the absolute magnitude of the deduced mixing ratios depends directly upon the choices made. The inference technique is not dependent upon any one transmittance model or any one temperature or pressure assumption.

The transmittance model of reference 10 was used to develop the inference technique, since it was available in program form. The relative merit of transmittance models is difficult to determine and is not the subject of this paper even though it is realized that the transmittance model does affect the absolute magnitude of the inferred mixing ratio. The versatility and ease of application of the technique of reference 10 contribute to its wide acceptance.

Temperatures and pressures as a function of altitude were taken from the 1962 U.S. Standard Atmosphere (ref. 11) for the development of the inference technique. In the implementation of the inference technique, model atmospheric temperatures and pressures near the geographic location of the measurement, or actual applicable data from the rawinsonde balloon network and the Meteorological Rocket Network, could be sources for temperatures and pressures. Use of temperatures obtained from the technique outlined in reference 3 is also possible.

Clouds, since they represent a boundary term in the integration, cannot be considered. In implementation of the technique, care must be used to be sure that the radiance data come either from clear locations or from above the clouds.

Inference at H_0.- The iterative technique to obtain mixing ratio begins at the highest tangent height H_0 where radiance information is available and then proceeds

downward in tangent height. This technique of solution is basically the solution of equation (4) for every line of sight, that is, for every tangent height.

The evaluation of equation (4) to obtain the calculated radiance $N_c(H_o)$ starts with the initial estimate that at H_o and above, the mixing ratio has a constant value w_o. The calculated radiance is subtracted from the measured radiance for that altitude to obtain a radiance error of

$$\Delta N(H_o) = N_m(H_o) - N_c(H_o)$$

The initial estimate of mixing ratio is corrected by

$$\Delta w = w \frac{\Delta N}{N_c}$$

Reasons for the choice of this linear relationship are shown later.

Once an initial estimate for Δw has been obtained, a new mixing ratio $w' = w + \Delta w$ may be used to compute a new calculated radiance N_c'. Now the derivative $\frac{dw}{dN}$ can be approximated by $\frac{dw}{dN} = \frac{w' - w}{N_c' - N_c}$.

The next estimate for change in mixing ratio is given by

$$\Delta w' = \Delta N' \frac{w' - w}{N_c' - N_c} \tag{7}$$

This last relationship is used repeatedly until the value of ΔN is within an acceptable criteria. The final value of mixing ratio is then assigned to the altitudes above H_o.

Inference below H_o.- For the lines of sight below H_o, equation (5) gives a clearer picture of the technique. A radiance is calculated from equation (5), and, by assuming that w in the new layer is the same as that in the layer above, the radiance error is formed as before:

$$\Delta N(H_i) = N_m(H_i) - N_c(H_i) \tag{8}$$

where the subscript i denotes a specific tangent height H. A relationship is needed to estimate the change in mixing ratio of the new layer which will change $N_c(H_i)$ and force $\Delta N(H_i)$ to become small. The values of temperature, pressure, and mixing ratio as a function of altitude are known up to the location of τ_3 (fig. 1) so that the first integral can be evaluated and stored. The second integral, containing the fractional contribution $G(H)$ (eq. (6)), gives the new information for the individual line of sight. The third integral changes slightly as a function of the mixing ratio in the second integral. The

radiance from the second integral is

$$N = -\int_{\nu} \int_{\tau_3}^{\tau_2} N_\nu(T)\, d\tau\, d\nu \tag{9}$$

Consider the temperature to be constant from τ_3 to τ_2 and the spectral interval to be small; then,

$$N = N_\nu(\tau_3 - \tau_2)\,\Delta\nu = N_\nu\,\Delta\tau\,\Delta\nu$$

If a new mixing ratio is assumed from τ_3 to τ_2, then

$$N' = N_\nu\,\Delta\nu\,\Delta\tau'$$

The fractional change in radiance is

$$\frac{N - N'}{N} = \frac{\Delta\tau - \Delta\tau'}{\Delta\tau} \tag{10}$$

Transmittance is a smoothly varying function of the amount of absorbing gas in the path considered. For small variations in the amount of absorbing gas, the linear relationship of

$$\tau = cws$$

is reasonable. If τ is differentiated with respect to s and the result substituted into equation (10), then

$$\frac{N - N'}{N} = \frac{cw\,\Delta s - cw'\,\Delta s}{cw\,\Delta s} = \frac{w - w'}{w}$$

or, since $w - w'$ is the change in mixing ratio,

$$\Delta w = \frac{N - N'}{N} w \tag{11}$$

Since $N - N'$ is approximately the change in $N_c(H_i)$ caused by changing w, the radiance error (eq. (8)) is equated to $N - N'$ and combined into equation (11) to yield the change in mixing ratio needed to make $\Delta N(H_i)$ small. The radiance is linearly related to mixing ratios for small changes of mixing ratio in the interval τ_3 to τ_2 by

$$\Delta w = \frac{\Delta N(H_i) w}{\int_{\nu} \int_{\tau_3}^{\tau_2} N_\nu(T)\, d\tau\, d\nu} \tag{12}$$

After this initial estimate, equation (7) is used to iterate until ΔN is small. The technique then proceeds to the next lower tangent height and repeats the iteration again.

Convergence criteria.- In this investigation a solution to equation (8) is considered to have been determined when $\Delta N(H_i)$ is sufficiently small and when any one of the following three conditions have been met: $|\Delta w| \leq 0.02\ w$; $|\Delta w| \leq 10^{-4}$ g/kg; and $|\Delta N| \leq 10^{-2}$ W/m^2-sr. These choices are an attempt to obtain sufficient accuracy in a minimum of computing time.

EVALUATION OF TECHNIQUE

The inference technique has been developed to deduce the mixing ratio of the emitting gas from a measured horizon radiance profile when the temperature and pressure as a function of altitude are known. In other words, the temperature, pressure, and radiance as a function of altitude along with an initial assumption about the mixing ratio are the inputs to the program; the output is the deduced mixing ratio of water vapor.

An evaluation of the iteration technique can be made when a consistent set of data exists, that is, when the temperature, pressure, altitude, mixing ratio, and radiance are uniquely related through the transmission model. It is then possible to perturb the inputs to the iteration technique in such a manner as to focus attention on the effects caused by specific errors in the deduced mixing-ratio output.

Reference-Data Set

In order to calculate a "measured" radiance profile, a mixing ratio as a function of altitude is necessary. No one mixing-ratio structure has been widely accepted; therefore, for purposes of analysis, a structure that was not completely unrealistic was assumed as a reference mixing ratio. It was assumed that above an altitude of 30 km the mixing ratio increased to 35 km and then remained constant from there to the top of the sensible atmosphere.

The radiance profile for 315 cm^{-1} to 475 cm^{-1} was computed from equation (4) by using the temperature and pressure from the 1962 U.S. Standard Atmosphere (table I) and the reference mixing-ratio structure. Values of the reference mixing ratio, along with the corresponding values of the reference radiance profile, are given in table II. This calculated radiance profile, also shown in figure 3, is considered to be part of the basic reference data required to evaluate the technique and is designated as a "measured" radiance profile for error discussions.

When the trends of the density (or pressure), temperature, and mixing ratio with altitude are known, the shape of the calculated and, thus, the measured radiance profile can be explained. In calculating the radiance shown in figure 3, for example, at altitudes

from 35 km to 30 km, the mixing ratio and temperature are decreasing; but the increasing density of the atmosphere is a stronger factor and thus the radiance increases. For altitudes between 30 km and 20 km, the density continues to increase, the mixing ratio remains constant, and the slope of the radiance profile increases, even though the temperature continues to decrease. Below 18 km the mixing ratio, the temperature, and the density all increase together, and the radiance profile increases rapidly until opacity is approached.

The radiance calculated by using the reference mixing ratio was used as the measured radiance input to the iteration program. Figure 4 shows that the deduced mixing ratio agrees very well with the reference mixing ratio; in fact, this agreement is a measure of the accuracy of the iteration with the given convergence criteria since the assumption of a constant mixing ratio above H_0 is completely compatible with the reference mixing ratio when H_0 = 35 km.

The sensitivity of the inference technique for water-vapor mixing ratio can be directly examined by perturbing the programed input data and examining the resulting output data. The following effects were examined: the effect of the requirement of the method to assume a constant mixing ratio above H_0; and the effects of radiance errors, tangent-height errors, pressure errors, and temperature errors. Errors associated with the choice of a transmission model were not investigated in this study.

Effect of Assumption of Constant Mixing Ratio Above H_0

The inference technique, as discussed previously, assumes that the mixing ratio from H_0 to the top of the sensible atmosphere is a constant and that this constant is the mixing ratio deduced at H_0. To evaluate this effect, the reference-data mixing ratio was perturbed as shown in table II by continuing the slope established between 30 km and 35 km to 40 km and then remaining constant at that value for higher altitudes. The calculated radiance values using this perturbation are also presented in table II. This radiance profile is now the measured input to the inference technique, but H_0 is still taken to be 35 km. Since the inference technique assumes that the mixing ratio is constant above H_0, the inferred results (see fig. 4 also) show that the error in the deduced mixing ratio is largest at high altitudes where the radiance increases, since the larger amounts of water vapor in the line of sight compose a greater percentage of the total radiance; the error decreases as the tangent height decreases since the percentage of influence of the water vapor above H_0 decreases as tangent height decreases.

Effects of Specific Errors

Radiance errors.- A scale perturbation in the measured radiance (fig. 5(a)) of ±4 percent resulted in a mixing ratio with the same basic shape as the initially assumed

mixing ratio, but shifted to higher or lower values. The large changes in the slope of inferred mixing ratio occur at the correct altitudes. In a precise measurement, radiance errors of ±1 percent in scale are possible at the present time.

A bias error in the measured radiance (fig. 5(b)) of ±0.1 W/m^2-sr has a large effect on the inferred mixing ratio at the higher altitudes. The radiance error is ±60 percent of measured radiance at H = 35 km. At H = 10 km the radiance error is only ±1.5 percent of the measured radiance, and the mixing-ratio error is small. In a precise measurement, bias errors of 0.01 W/m^2-sr are possible at the present time.

Errors in mixing ratio due to noise radiance errors are shown in figure 5(c). Random errors with a mean of zero and a standard deviation of 0.02 W/m^2-sr were used to perturb the measured radiance. The errors mask the true structure of mixing-ratio changes and are larger at high altitudes where the radiance error is a larger percentage of the measured radiance. Noise radiance errors of 0.01 W/m^2-sr are possible in a precise measurement at the present time.

Tangent-height errors.- Effects due to tangent-height errors are evident in figure 5(d). Errors in mixing ratio are much larger below h = 30 km than above. Altitudes at which major changes occur in the inferred mixing ratio are in direct proportion to the tangent-height error. The magnitude of the inferred mixing-ratio error increases steadily at the lower altitudes.

Pressure errors.- Errors that would result in deduced mixing ratios because of an incorrect knowledge of the applicable pressures are illustrated in figure 5(e). A pressure that is assumed to be a constant percentage, whether high or low (±10 percent in fig. 5(e)), results in a scale-type error. A comparison of figures 5(a) and 5(e) illustrates this effect. Inferred mixing ratios change sharply at the correct altitudes.

Temperature errors.- Errors due to an incorrect knowledge of the temperature structure in the atmosphere are illustrated in figure 5(f). For the assumed errors of $\pm 5^{\circ}$ K, the inferred mixing ratio changes sharply at the correct altitude so that the basic shape of the mixing-ratio structure is retained even though the absolute values of the mixing ratio are shifted. An additive temperature error causes errors in deduced mixing ratios that are similar to, but not directly comparable with, scale errors, since both the Planck function and the transmission function in equation (5) are affected by the change in temperature.

Limitation of Present Technique

The errors presented in tangent height, pressure, and temperature are not felt to be unreasonable. In implementation of the technique, both a lack of knowledge of the applicable temperature and pressure and the errors in tangent height would probably cause larger errors in the inferred mixing ratio than the errors in radiance measurements.

The present work has been constrained to the one transmittance model discussed in reference 10. Future efforts should use more accurate transmittance models as they become available. Spectral intervals other than the one used herein should be investigated to determine whether the technique could yield useful results to lower and higher altitudes. The present technique could also be evaluated for determining the mixing ratio of ozone in the 9.6μ band. Finally, future work should consider a realistic cloud model in order to investigate any information about clouds that can be deduced.

MIXING-RATIO INFERENCE FROM MEASURED HORIZON RADIANCE PROFILES

Horizon radiance profiles have been measured in the 315 cm^{-1} to 475 cm^{-1} spectral region in NASA's Project Scanner. This section contains a description of the data measured in the summer, meteorological conditions at the time of measurement, and the application of the mixing-ratio inference technique to the summer data.

Measured Horizon Radiance Profiles

The horizon radiance profiles were measured on a rocket probe launched from the NASA Wallops Station at 0618 GMT on August 16, 1966 (ref. 1). Peak altitude attained in the flight was 620 km. Measured horizon radiance profiles were grouped into seven geographic cells which were centered at the following locations:

	Values for geographic cells –						
	1	2	3	4	5	6	7
Latitude, ^{o}N	58	53	47	43	35	21	17
Longitude, ^{o}W	68	60	57	45	48	55	60
Number of profiles . . .	7	8	3	5	12	9	6

The profiles for each cell were then averaged to obtain one measured radiance profile representative of each cell. The average measured radiance profile for each cell is given in table III. The radiance-measurement error of these data was approximately ±4 percent in scale and ±0.08 W/m^2-sr in bias. The standard deviation of noise radiance error was 0.08 W/m^2-sr for each radiance profile. The noise error for the average measured radiance profile for each cell is dependent on the number of profiles in the cell and will decrease with the square root of the number of profiles in the cell. For example, the 12 profiles in cell 5 have a standard deviation of the noise-radiance error of 0.046 W/m^2-sr. Tangent-height errors are ±1.3 km. These radiance profiles suffer

from a frequency limitation of the measuring instrument as discussed in reference 1, and the data are suitable for inferring mixing ratio only down to about 12 km. This altitude is above the cloud heights that were measured independently.

Meteorological Data

In the Project Scanner experiment an attempt was made to determine the atmospheric temperature and pressure near the time of and in the location where radiance profiles were measured. Atmospheric data for each geographic cell are given in table IV. A discussion of the data used in developing these atmospheres is given in appendix B of reference 1. Balloon data of temperature and pressure were used from the surface to an altitude of 30 km or as high as data were available. The exact location of each cell given previously was determined by the available balloon data. Cell 6 was assumed to have the same data as was measured from the balloon in cell 7. Above an altitude of 30 km, temperatures were estimated from the wind and temperature measurements made by rocketsondes at Fort Churchill, Canada, Wallops Island, Va., and White Sands Missile Range, New Mexico. (Wind data were not obtained at White Sands.) If balloon temperature data ceased before $h = 30$ km, the temperature was linearly interpolated to the estimated temperature at 30 km. Pressures for altitudes above the 30-mb level were calculated by hydrostatic buildup by using the pressure at the 30-mb level as a base since pressures below that altitude were available from the balloon measurements (1 bar equals 1×10^5 N/m^2). Water-vapor mixing ratio was measured as a part of the balloon system for the cells for altitudes varying between 3 and 10 km.

Inferred Water-Vapor Mixing Ratios

The water-vapor mixing ratios deduced by using the inference technique from the measured radiance profiles in table III are given in table V. Figure 6 shows two of the mixing-ratio profiles (cells 1 and 5) along with data obtained from rawinsonde balloons for those latitudes near the time of the Scanner launch. The inferred and balloon data do not overlap in altitude; however, they do appear to be compatible. Some of the more recently reported measurements of mixing ratios in the stratosphere (refs. 4 and 12) are also shown in figure 6. In the region where comparable measurements exist, the mixing ratios inferred with this technique are within factors of 2 to 4 of other measurements. Since all the data in the seven cells were measured within approximately 15 minutes, an examination of latitudinal variation of mixing ratio is possible.

Figure 7 (a plot of the data in table V) shows there is no significant variation of mixing ratio with latitude above approximately 18 km. Below 18 km a significant variation of mixing ratio does exist, reflecting the large variations of mixing ratio that are known to exist in the troposphere. Mixing ratio decreases with increasing latitude. In

all cells the mixing ratio decreases with altitude to a minimum at a point ranging from 3 km to 5 km above the tropopause altitude. Above an altitude of 20 km the mixing ratio shows a slight increase to 35 km. This comparison of mixing-ratio profiles as a function of latitude is more significant and accurate than is the absolute magnitude of the mixing ratios since approximately the same errors are present in all the data.

CONCLUDING REMARKS

A technique to infer atmospheric water-vapor mixing-ratio structure has been presented. The technique was implemented for the 315 cm^{-1} to 475 cm^{-1} spectral interval of the rotational band of water vapor. Accurate mixing ratios were inferred over the altitude range investigated (10 km to 35 km) when the technique input data contained no errors. The radiance input errors of scale, bias, and noise were demonstrated and were found to be less significant than tangent-height errors, temperature errors, and pressure errors.

Water-vapor mixing ratios were inferred by using measured horizon radiance profiles from the NASA Project Scanner flight conducted in August 1966. No significant latitudinal variation existed above an altitude of 18 km. Below 18 km a latitudinal variation does exist that is consistent with the large variations that are known to exist in the troposphere. The mixing ratio decreases with altitude to a minimum at a point ranging from 3 km to 5 km above the tropopause altitude. Above an altitude of 20 km the mixing ratio shows a slight increase to 35 km.

Langley Research Center,
National Aeronautics and Space Administration,
Langley Station, Hampton, Va., March 19, 1969,
715-02-00-01-23.

REFERENCES

1. McKee, Thomas B.; Whitman, Ruth I.; and Davis, Richard E.: Infrared Horizon Profiles for Summer Conditions From Project Scanner. NASA TN D-4741, 1968.

2. Whitman, Ruth I.; McKee, Thomas B.; and Davis, Richard E.: Infrared Horizon Profiles for Winter Conditions From Project Scanner. NASA TN D-4905, 1968.

3. McKee, Thomas B.; Whitman, Ruth I.; and Lambiotte, Jules J., Jr.: A Technique to Infer Atmospheric Temperature From Horizon Radiance Profiles. NASA TN D-5068, 1969.

4. Mastenbrook, H. J.: Water Vapor Distribution in the Stratosphere and High Troposphere. J. Atmos. Sci., vol. 25, no. 2, Mar. 1968, pp. 299-311.

5. Williamson, E. J.; and Houghton, J. T.: Radiometric Measurements of Emission From Stratospheric Water Vapor. Quart. J. Roy. Meteorol. Soc., vol. 91, no. 389, July 1965, pp. 330-338.

6. Conrath, Barney J.: On a Mathematical Formulation of the Constituent Inversion Problem for Planetary Atmospheres. NASA GSFC Doc. X-622-66-542, Oct. 1966.

7. Yamamoto, G.; and Tanaka, M.: Estimation of Water Vapor Distribution in the Atmosphere From Satellite Measurements. Application Satellites. P. Contensou, G. N. Duboshin, and W. F. Hilton, eds., Gordon and Breach, Inc., 1967, pp. 253-268.

8. Goody, R. M.: Atmospheric Radiation I. – Theoretical Basis. Clarendon Press (Oxford), 1964.

9. Bates, Jerry C.; Hanson, David S.; House, Fred B.; Carpenter, Robert O'B.; and Gille, John C.: The Synthesis of 15μ Infrared Horizon Radiance Profiles From Meteorological Data Inputs. NASA CR-724, 1967.

10. Elsasser, Walter M.; and Culbertson, Margaret F.: Atmospheric Radiation Tables. Meteorol. Monogr., vol. 4, no. 23, Aug. 1960.

11. Anon.: U.S. Standard Atmosphere, 1962. NASA, U.S. Air Force, and U.S. Weather Bur., Dec. 1962.

12. Neporent, B. S.; Kiseleva, M. S.; Makogonenko, A. G.; and Shlyakhov, V. I.: Determination of Moisture in the Atmosphere From Absorption of Solar Radiation. Appl. Opt., vol. 6, no. 11, Nov. 1967, pp. 1845-1850.

TABLE I.- U.S. 1962 STANDARD ATMOSPHERE VALUES

[See ref. 11]

Altitude, km	Temperature, °K	Pressure, mb
0	288.15	1013.25
2	275.15	795.01
4	262.17	616.60
6	249.19	472.18
8	236.22	356.52
10	223.25	265.00
12	216.65	193.99
14	216.65	141.70
16	216.65	103.53
18	216.65	75.65
20	216.65	55.29
22	218.57	40.47
24	220.56	29.72
26	222.54	21.88
28	224.53	16.16
30	226.51	11.97
32	228.49	8.89
34	233.75	6.63
36	239.28	4.99
38	244.82	3.77
40	250.35	2.87
42	255.88	2.20
44	261.40	1.70

TABLE II.- MIXING RATIOS AND CALCULATED RADIANCE PROFILES

(a) Reference-data set

Altitude, km	Mixing ratio, g/kg	Tangent height, km	Calculated radiance, W/m^2-sr
0	5.0×10^0	0	11.01
1	3.0	1	10.96
2	1.8	2	10.91
3	1.0	3	10.86
4	6.0×10^{-1}	4	10.79
5	3.5	5	10.68
6	2.2	6	10.44
7	1.3	7	9.94
8	7.6×10^{-2}	8	9.05
9	4.5	9	7.83
10	2.7	10	6.48
11	1.6	11	5.27
12	1.0	12	4.33
13	9.0×10^{-3}	13	3.77
14	8.0	14	3.24
15	7.1	15	2.77
16	6.3	16	2.35
17	5.6	17	2.00
18	5.0	18	1.70
19	5.0	19	1.48
20	5.0	20	1.29
21	5.0	21	1.13
22	5.0	22	.98
23	5.0	23	.85
24	5.0	24	.73
25	5.0	25	.62
26	5.0	26	.53
27	5.0	27	.46
28	5.0	28	.39
29	5.0	29	.34
30	5.0	30	.29
31	6.3	31	.27
32	7.8	32	.25
33	9.8	33	.22
34	1.2×10^{-2}	34	.19
35	1.5	35	.17
36	1.5		
37	1.5		
38	1.5		
39	1.5		
40	1.5		
41	1.5		
42	1.5		
43	1.5		
44	1.5		
45	1.5		

(b) Perturbed-data set

Altitude, km	Mixing ratio, g/kg	Tangent height, km	Calculated radiance, W/m^2-sr
0	5.0×10^0	0	11.00
1	3.0	1	10.96
2	1.8	2	10.91
3	1.0	3	10.86
4	6.0×10^{-1}	4	10.79
5	3.5	5	10.68
6	2.2	6	10.44
7	1.3	7	9.94
8	7.6×10^{-2}	8	9.05
9	4.5	9	7.84
10	2.7	10	6.49
11	1.6	11	5.29
12	1.0	12	4.36
13	9.0×10^{-3}	13	3.80
14	8.0	14	3.28
15	7.1	15	2.81
16	6.3	16	2.39
17	5.6	17	2.04
18	5.0	18	1.74
19	5.0	19	1.53
20	5.0	20	1.34
21	5.0	21	1.18
22	5.0	22	1.03
23	5.0	23	.90
24	5.0	24	.78
25	5.0	25	.68
26	5.0	26	.59
27	5.0	27	.51
28	5.0	28	.45
29	5.0	29	.40
30	5.0	30	.35
31	6.3	31	.34
32	7.8	32	.31
33	9.8	33	.30
34	1.2×10^{-2}	34	.28
35	1.5	35	.26
36	1.85		
37	2.3		
38	2.8		
39	3.5		
40	4.4		
41	4.4		
42	4.4		
43	4.4		
44	4.4		
45	4.4		

TABLE III.- MEASURED RADIANCE PROFILES FROM THE PROJECT SCANNER FLIGHT IN AUGUST 1966

[Data from ref. 1; 375 cm^{-1} to 475 cm^{-1} spectral interval]

Tangent height, km	Radiance profiles, W/m^2-sr, for cell –						
	1	2	3	4	5	6	7
10	6.57	6.27	6.02	6.11	7.01	7.18	7.74
11	5.52	5.38	5.23	5.51	6.32	6.26	6.79
12	4.47	4.53	4.45	4.88	5.54	5.31	5.75
13	3.66	3.82	3.76	4.25	4.72	4.41	4.71
14	3.12	3.28	3.21	3.64	3.93	3.64	3.74
15	2.76	2.86	2.78	3.09	3.22	3.00	2.92
16	2.48	2.52	2.44	2.63	2.65	2.49	2.31
17	2.24	2.25	2.18	2.29	2.22	2.11	1.89
18	2.02	2.03	1.96	2.04	1.92	1.83	1.64
19	1.84	1.84	1.76	1.84	1.71	1.61	1.48
20	1.67	1.64	1.58	1.68	1.54	1.43	1.36
21	1.48	1.46	1.42	1.52	1.40	1.29	1.25
22	1.29	1.29	1.26	1.37	1.27	1.16	1.12
23	1.14	1.15	1.10	1.22	1.12	1.05	.99
24	1.02	1.02	.95	1.09	.99	.95	.88
25	.91	.90	.82	.99	.87	.85	.79
26	.81	.80	.74	.90	.78	.76	.68
27	.70	.70	.67	.82	.70	.66	.61
28	.61	.61	.61	.74	.63	.58	.56
29	.54	.52	.58	.67	.56	.51	.50
30	.48	.45	.53	.60	.51	.46	.44
31	.43	.40	.47	.54	.46	.42	.42
32	.38	.36	.40	.47	.42	.39	.38
33	.32	.31	.32	.40	.36	.35	.34
34	.28	.27	.27	.35	.32	.31	.29
35	.24	.23	.24	.32	.29	.26	.24

TABLE IV.- MODEL ATMOSPHERES DERIVED FROM METEOROLOGICAL DATA

[From ref. 1]

Altitude, km	Cell 1 (58° N 68° W)		Cell 2 (53° N 60° W)		Cell 3 (47° N 57° W)		Cell 4 (43° N 45° W)	
	Temperature, °K	Pressure, mb	Temperature, °K	Pressure, mb	Temperature, °K	Pressure, mb	Temperature, °K	Pressure, mb
0	288.0	1010.000	288.0	1010.000	286.0	1012.000	294.0	1025.000
2	277.0	800.511	277.4	800.575	280.1	807.089	284.3	811.321
4	263.2	626.923	264.2	625.462	268.4	634.169	278.2	637.879
6	250.9	477.778	251.3	477.778	257.3	485.542	260.8	489.881
8	234.7	362.245	237.1	364.762	243.3	371.429	246.5	375.253
10	221.7	267.500	221.7	268.487	230.0	277.642	231.3	281.707
12	224.9	196.296	223.8	196.543	217.1	203.652	213.9	207.343
14	224.0	145.370	221.2	145.000	218.0	149.000	213.1	148.810
16	224.0	111.025	222.7	106.884	218.0	110.075	216.5	105.932
18	224.3	79.783	224.0	79.690	219.6	80.161	219.5	81.053
20	225.0	59.065	225.0	59.039	223.1	56.319	222.0	59.115
22	225.6	43.153	225.9	42.702	224.6	43.495	222.6	43.420
24	227.6	31.922	226.0	31.787	225.8	32.132	223.0	31.998
26	232.0	23.590	227.0	23.475	227.2	23.761	225.2	23.583
28	233.6	17.715	228.3	17.491	230.6	17.690	228.1	17.676
30	235.0	13.200	235.0	12.950	237.0	13.170	232.7	13.151
32	237.8	9.910	237.0	9.720	237.0	9.900	238.0	9.740
34	240.6	7.470	240.0	7.320	240.0	7.450	241.0	7.340
36	245.6	5.650	244.0	5.530	245.0	5.640	246.0	5.560
38	252.8	4.310	251.0	4.210	251.0	4.290	250.0	4.240
40	260.0	3.310	258.0	3.230	257.0	3.290	256.0	3.240
42	262.8	2.556	261.0	2.490	260.0	2.535	260.0	2.498
44	256.6	1.971	264.0	1.920	263.0	1.959	263.0	1.930
46	267.0	1.523	265.0	1.491	265.0	1.517	265.0	1.495
48	266.0	1.183	264.0	1.156	265.0	1.177	264.0	1.159
50	265.0	.918	263.0	.895	262.0	.911	262.0	.897
52	261.4	.710	259.0	.691	260.0	.704	261.0	.694
54	258.8	.548	256.0	.532	257.0	.543	260.0	.536
56	257.5	.442	254.7	.431	255.0	.439	257.0	.433
58	256.3	.336	253.3	.331	253.0	.334	254.0	.331
60	255.0	.230	252.0	.230	251.0	.230	251.0	.228
62	246.2	.180	244.4	.180	243.8	.179	243.0	.178
64	237.4	.130	236.8	.130	236.6	.128	235.0	.128
66	229.0	.095	229.0	.095	229.0	.093	227.6	.093
68	221.0	.074	221.0	.074	221.0	.073	220.8	.073
70	213.0	.053	213.0	.053	213.0	.053	214.0	.053

TABLE IV.- MODEL ATMOSPHERES DERIVED FROM METEOROLOGICAL DATA – Concluded

[From ref. 1]

Altitude, km	Cell 5 (35° N 48° W)		Cell 6 (21° N 55° W)		Cell 7 (17° N 60° W)	
	Temperature, °K	Pressure, mb	Temperature, °K	Pressure, mb	Temperature, °K	Pressure, mb
0	299.0	1023.000	301.0	1016.000	301.0	1016.000
2	284.1	785.377	287.8	808.129	287.8	808.129
4	274.8	639.370	275.2	637.736	275.2	637.736
6	264.5	495.294	259.7	492.669	259.7	492.669
8	250.5	380.612	252.7	379.412	252.7	379.412
10	235.3	287.600	237.1	286.800	237.1	286.800
12	218.2	213.194	220.9	213.014	220.9	213.014
14	204.0	155.000	209.0	154.749	209.0	154.749
16	207.5	112.398	201.0	110.853	201.0	110.853
18	213.0	81.087	205.0	78.659	205.0	78.659
20	217.1	59.074	212.6	57.080	212.6	57.080
22	220.5	43.253	217.5	41.525	217.5	41.525
24	222.7	31.744	219.0	30.412	219.0	30.422
26	225.6	23.350	227.0	22.585	227.0	22.585
28	227.7	17.360	227.7	16.833	227.7	16.839
30	230.0	12.830	227.0	12.390	225.0	12.380
32	239.0	9.620	235.0	9.250	233.0	9.220
34	244.0	7.270	242.0	6.970	241.0	6.930
36	248.0	5.520	247.0	5.290	247.0	5.260
38	251.0	4.220	250.0	4.030	250.0	4.010
40	254.0	3.230	253.0	3.080	253.0	3.070
42	259.0	2.481	259.0	2.370	259.0	2.358
44	264.0	1.917	266.0	1.834	260.0	1.825
46	265.0	1.487	268.0	1.426	270.0	1.420
48	264.0	1.153	265.0	1.108	269.0	1.107
50	262.0	.893	262.0	.859	262.0	.859
52	265.0	.692	267.0	.666	268.0	.667
54	268.0	.538	273.0	.520	273.0	.520
56	264.0	.434	267.0	.422	266.3	.425
58	260.0	.329	261.0	.323	259.7	.330
60	256.0	.225	255.0	.225	253.0	.235
62	248.4	.181	247.8	.181	246.2	.189
64	240.8	.136	240.6	.136	239.4	.143
66	233.4	.102	233.2	.102	232.6	.108
68	226.2	.077	225.6	.077	225.8	.083
70	219.0	.053	218.0	.053	219.0	.058

TABLE V.- DEDUCED WATER-VAPOR MIXING RATIOS

Altitude, km	Mixing ratios, g/kg, for cell –						
	1	2	3	4	5	6	7
12	7.9×10^{-3}	8.6×10^{-3}	9.7×10^{-3}	15.6×10^{-3}	29.3×10^{-3}	22.9×10^{-3}	33.4×10^{-3}
13	5.4	6.8	7.2	13.3	27.6	19.5	26.8
14	4.3	5.7	5.9	11.4	20.9	17.0	20.4
15	3.9	5.0	5.1	9.2	13.4	14.0	14.1
16	3.9	4.6	4.7	6.5	9.3	10.7	9.2
17	4.1	4.5	4.7	5.3	6.6	8.5	6.0
18	4.4	4.8	4.9	5.0	5.4	7.0	4.8
19	4.9	5.2	5.2	5.1	5.1	6.0	4.4
20	5.7	5.5	5.3	5.7	5.3	5.5	4.8
21	6.2	6.0	5.6	6.5	6.0	5.8	5.7
22	5.8	6.0	6.1	6.9	6.5	5.9	5.9
23	5.8	6.4	6.1	7.0	6.5	6.5	6.0
24	6.2	6.7	5.7	7.1	6.6	6.9	6.1
25	6.5	7.1	5.2	7.8	6.5	7.0	6.2
26	7.0	7.9	5.5	8.7	6.9	7.5	5.4
27	6.8	8.4	5.7	9.6	7.6	7.6	6.1
28	7.0	8.6	6.0	9.7	8.3	8.2	7.7
29	7.5	7.9	8.1	10.9	8.1	7.9	7.9
30	7.8	7.2	9.8	12.1	9.1	8.4	7.6
31	9.4	8.4	12.2	14.2	10.0	9.6	10.5
32	10.7	10.2	12.9	14.7	11.9	12.2	12.5
33	10.8	11.1	11.2	14.4	12.2	14.6	16.2
34	13.2	13.6	12.3	17.0	16.3	17.0	17.0
35	15.8	16.1	16.1	22.3	19.4	19.3	18.3
Latitude, ^{o}N	58	53	47	43	35	21	17
Longitude, ^{o}W	68	60	57	45	48	55	60
Tropopause altitude, km	10	10	12	14	14	16	16

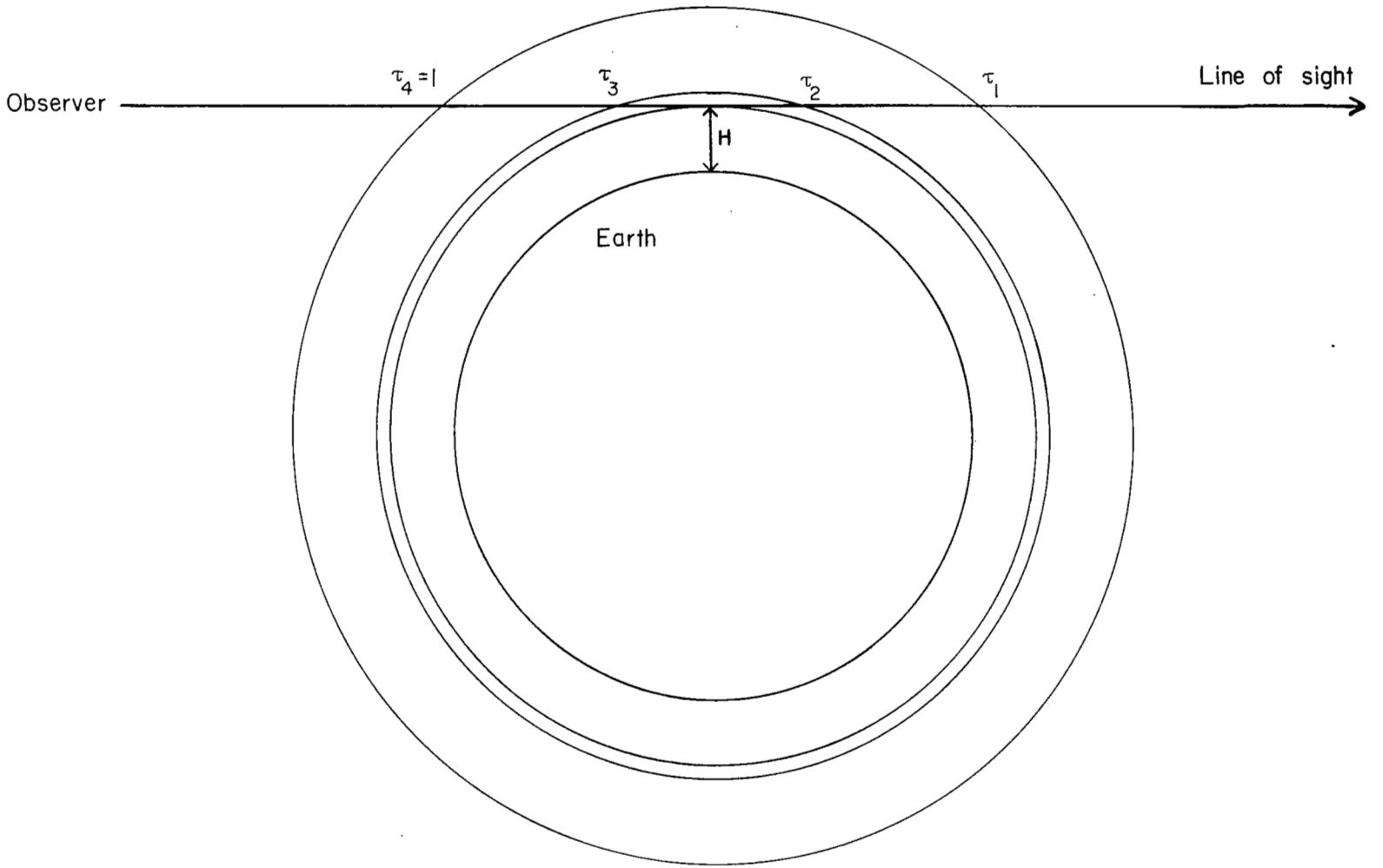

Figure 1.- Horizon geometry.

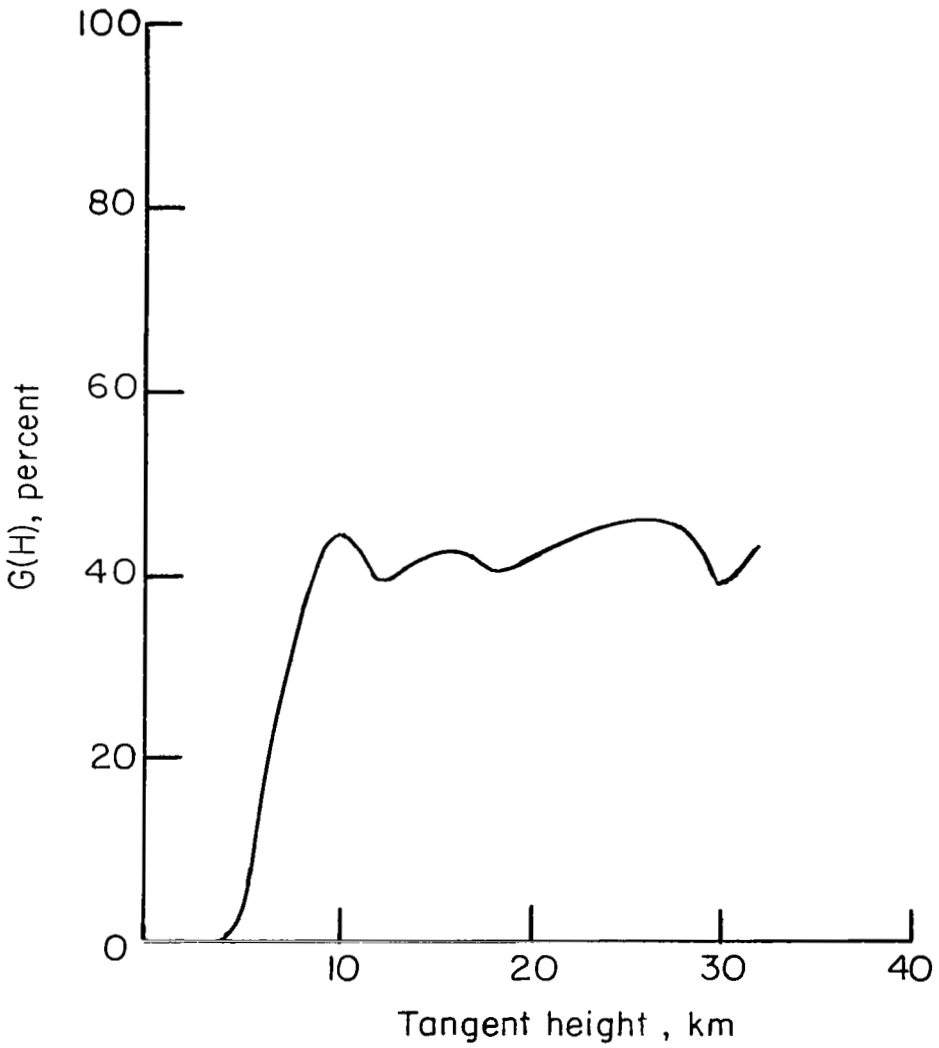

Figure 2.- Calculated radiance contribution from the 1-km-thick layer above the tangent point for the 315 cm^{-1} to 475 cm^{-1} spectral interval by using 1962 U.S. Standard Atmosphere and the reference mixing ratio.

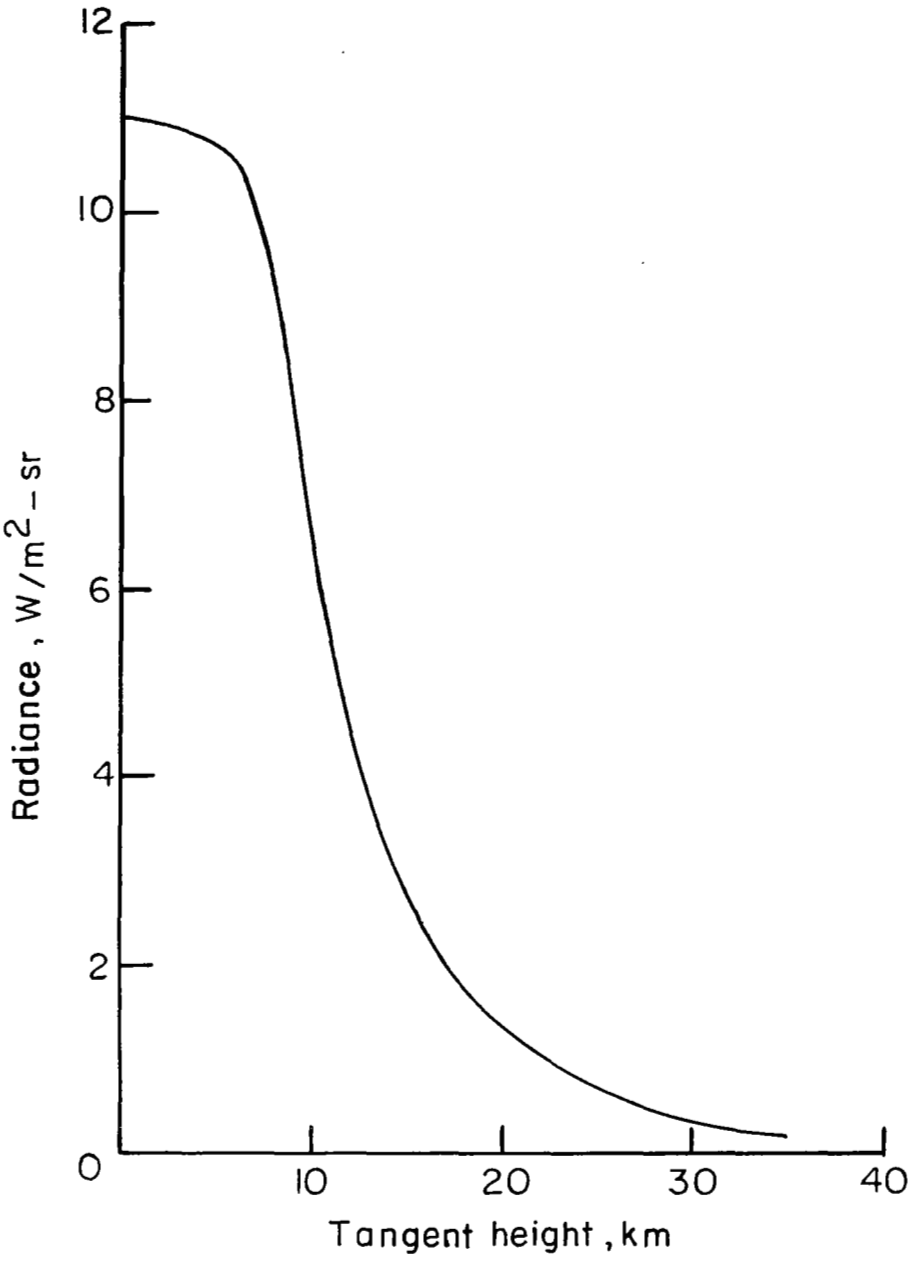

Figure 3.- Radiance profile for 315 cm^{-1} to 475 cm^{-1} spectral interval calculated by using 1962 U.S. Standard Atmosphere and the reference mixing ratio.

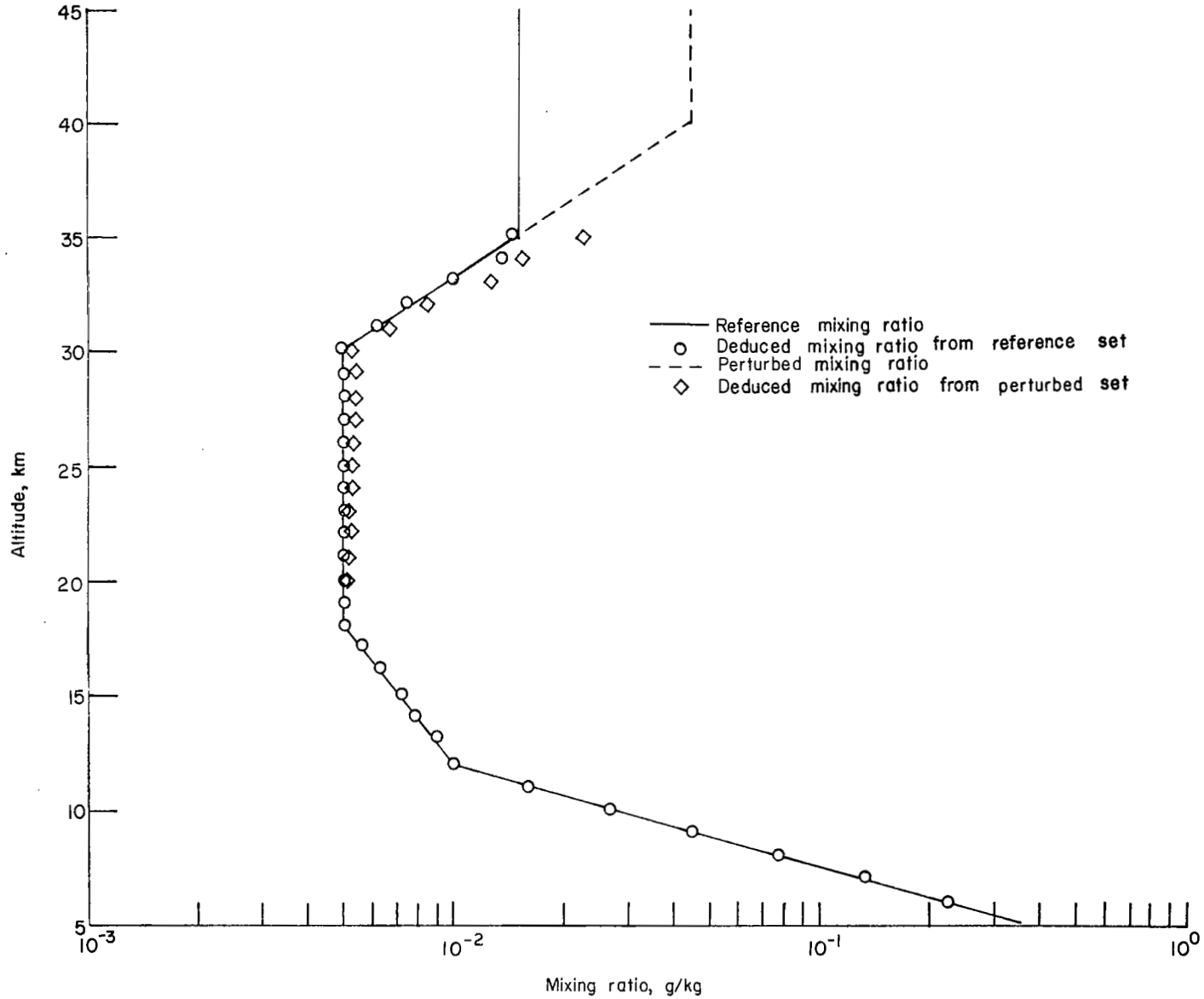

Figure 4.- Effect of errors in the initially assumed mixing ratio on the inferred mixing ratio.

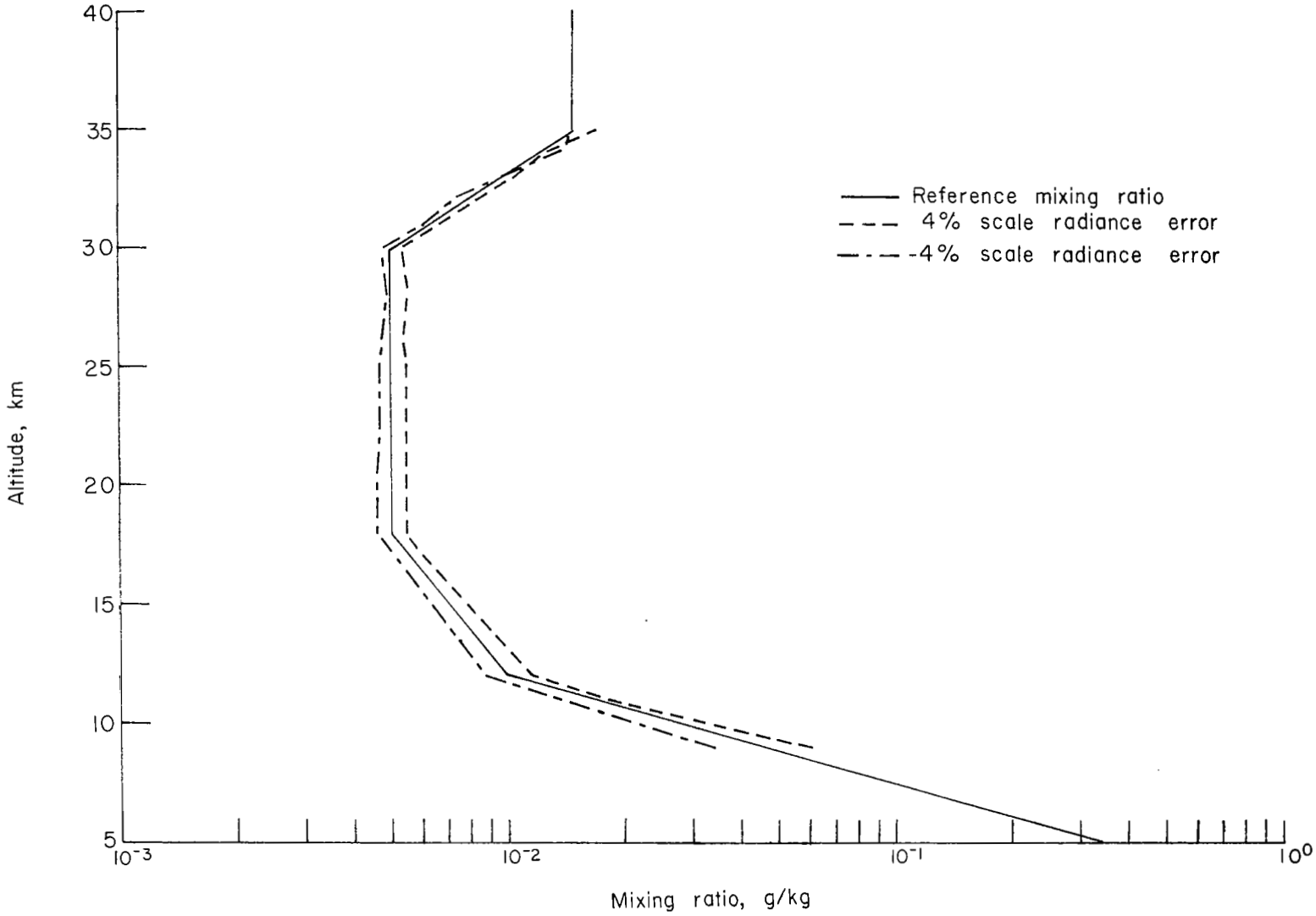

(a) Scale radiance error.

Figure 5.- Inferred mixing ratios for perturbed data.

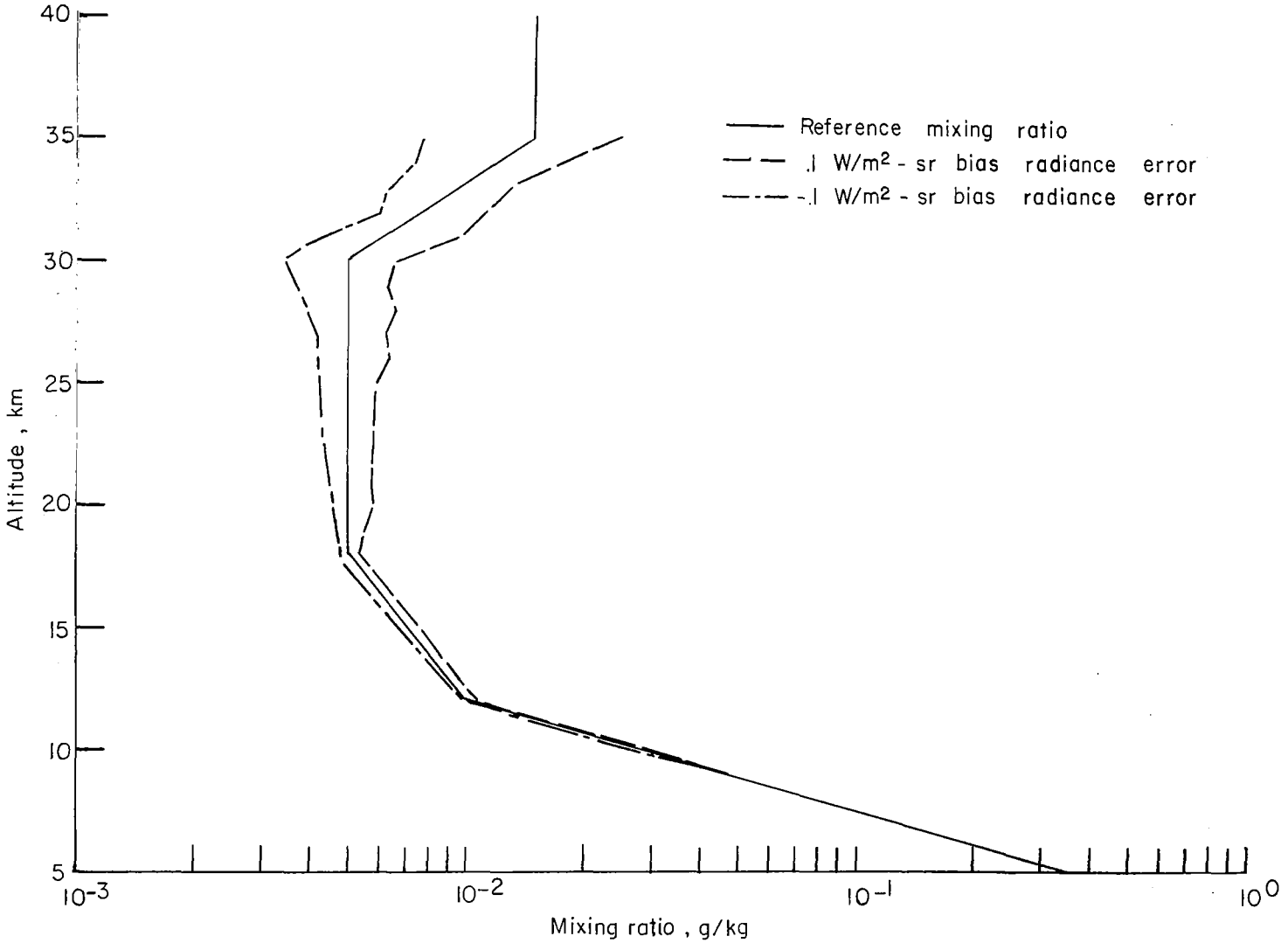

(b) Bias radiance error.

Figure 5.- Continued.

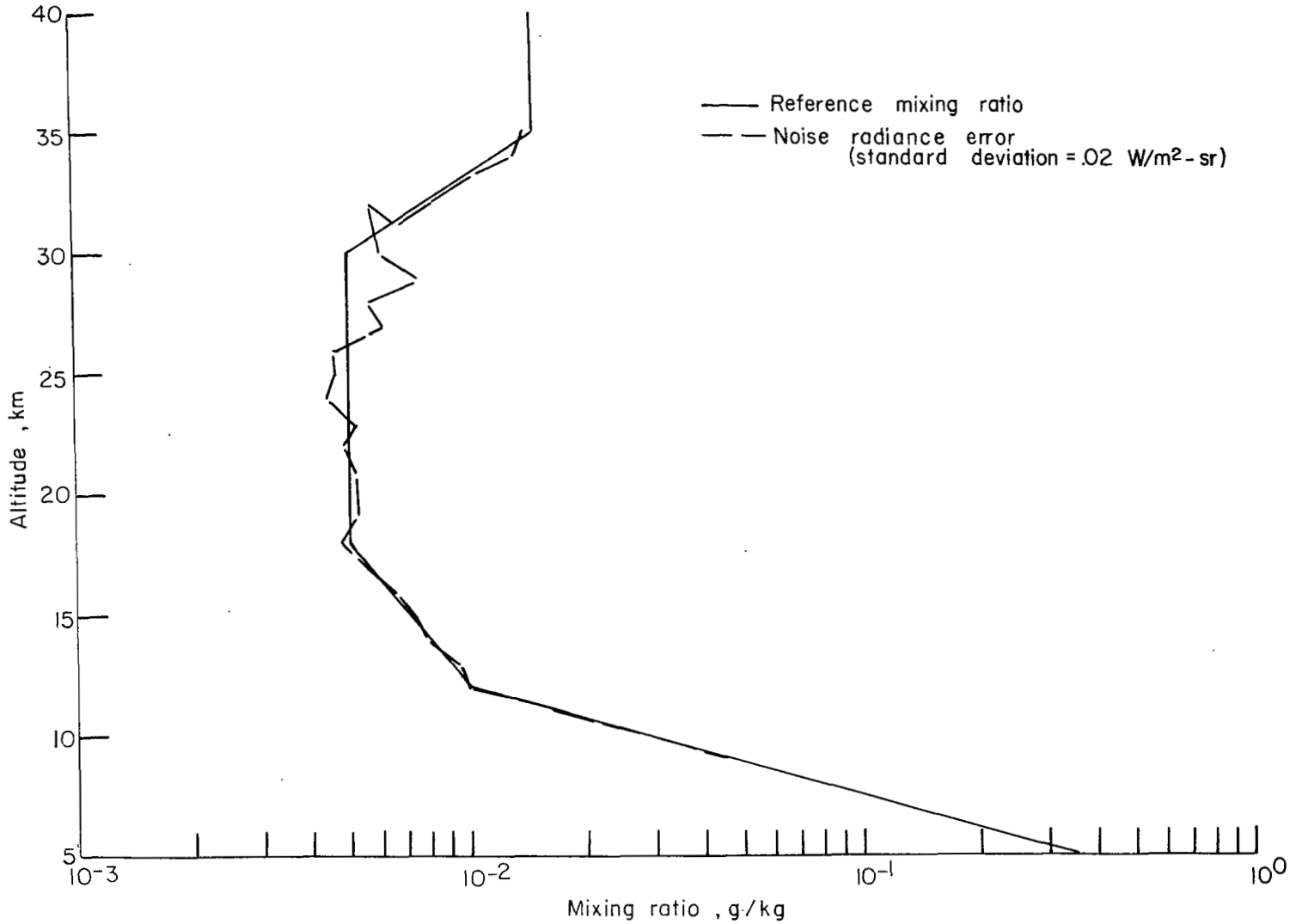

(c) Noise radiance error.

Figure 5.- Continued.

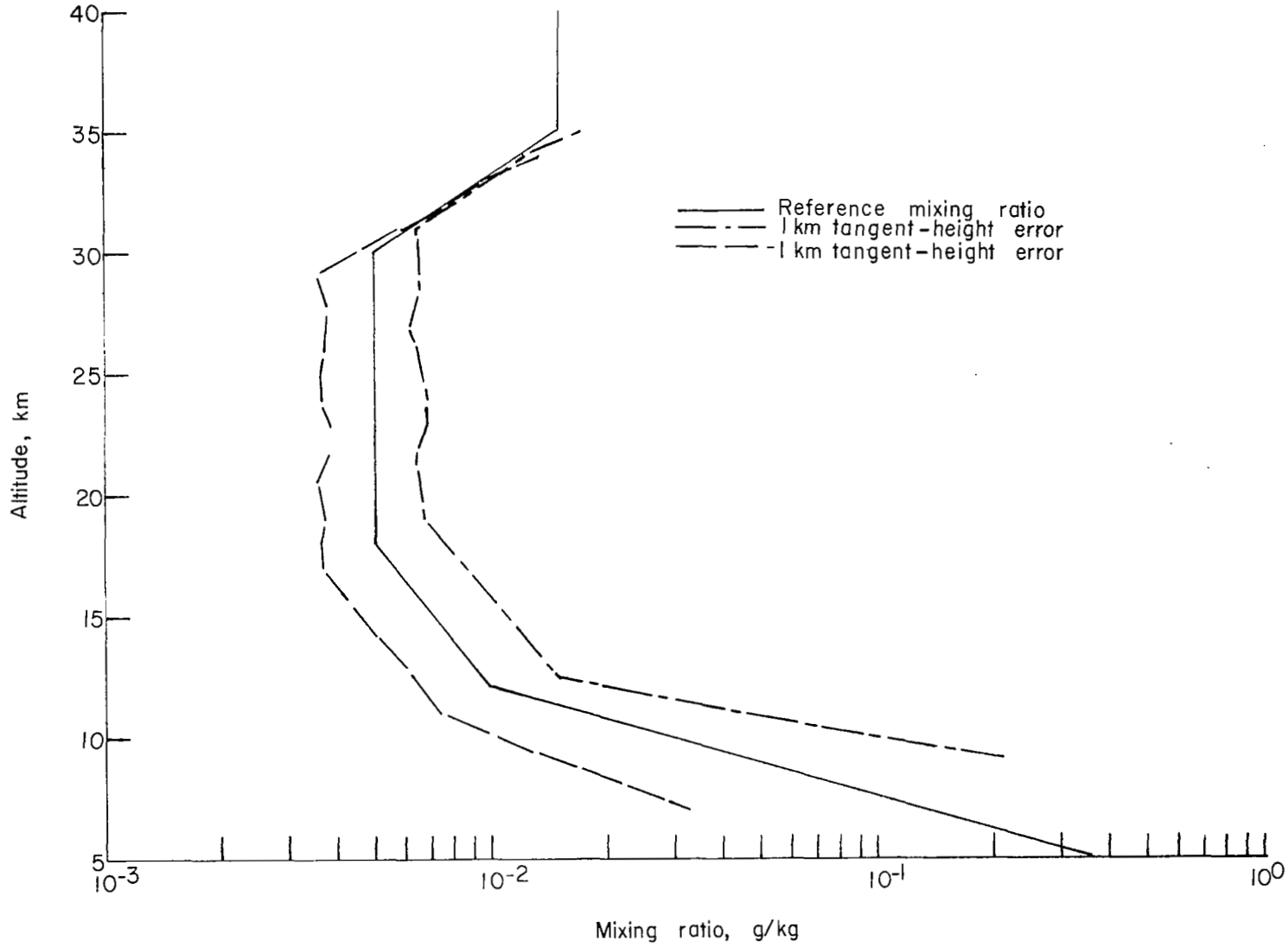

(d) Tangent-height error.

Figure 5.- Continued.

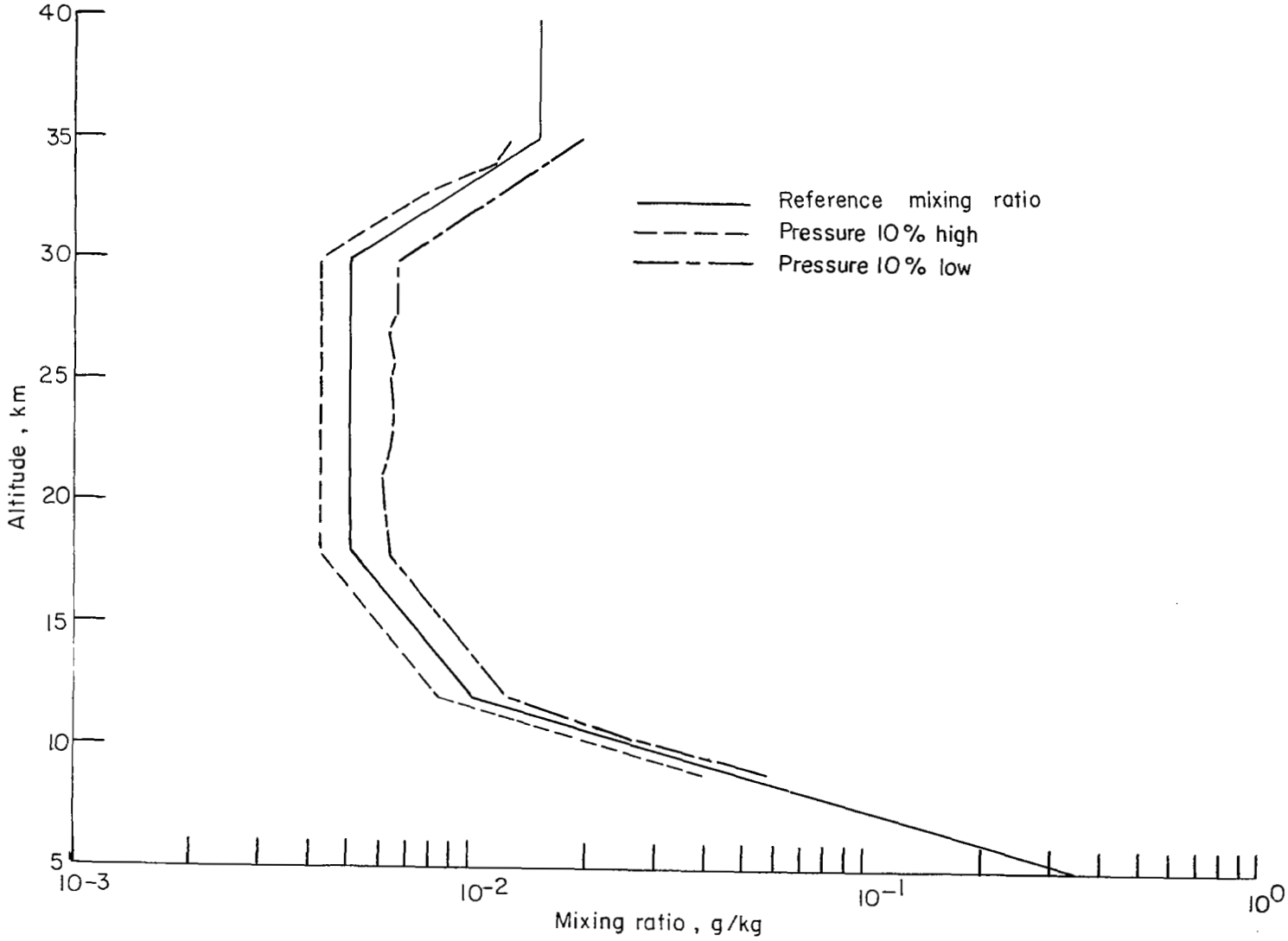

(e) Pressure error.

Figure 5.- Continued.

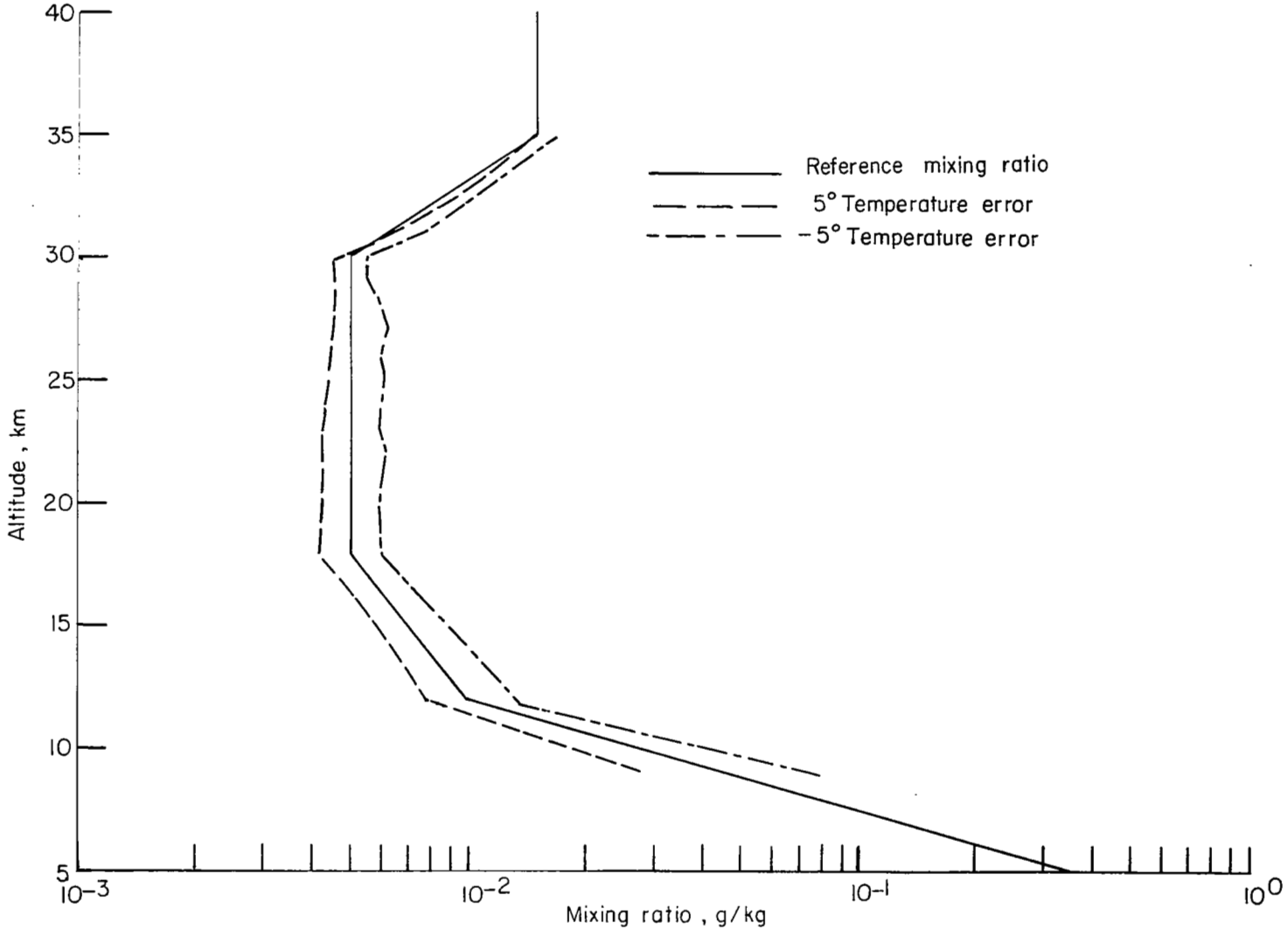

(f) Temperature error.

Figure 5.- Concluded.

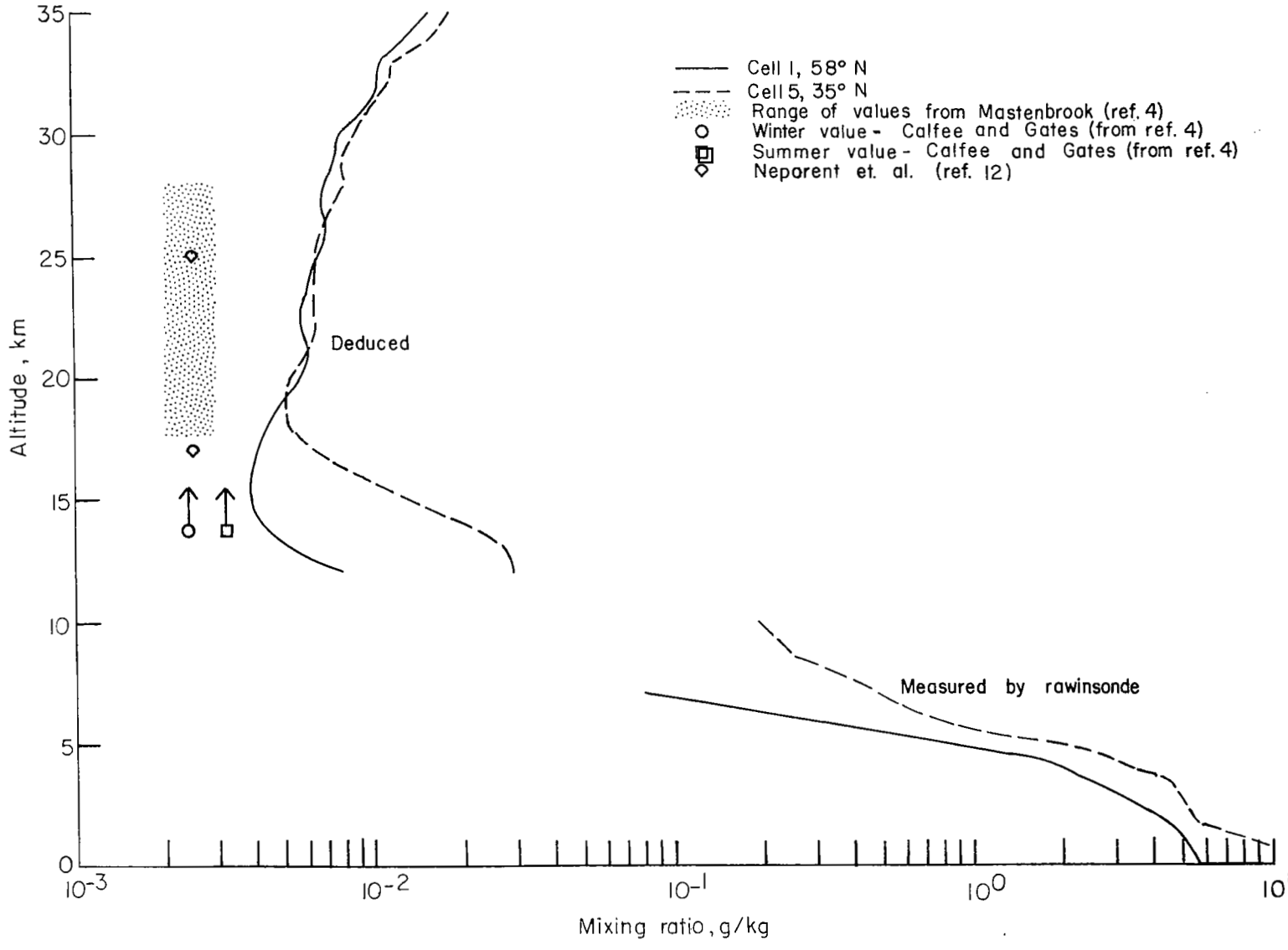

Figure 6.- Inferred and measured mixing ratios for cells 1 and 5 from Project Scanner data along with other measurements obtained from references 4 and 12.

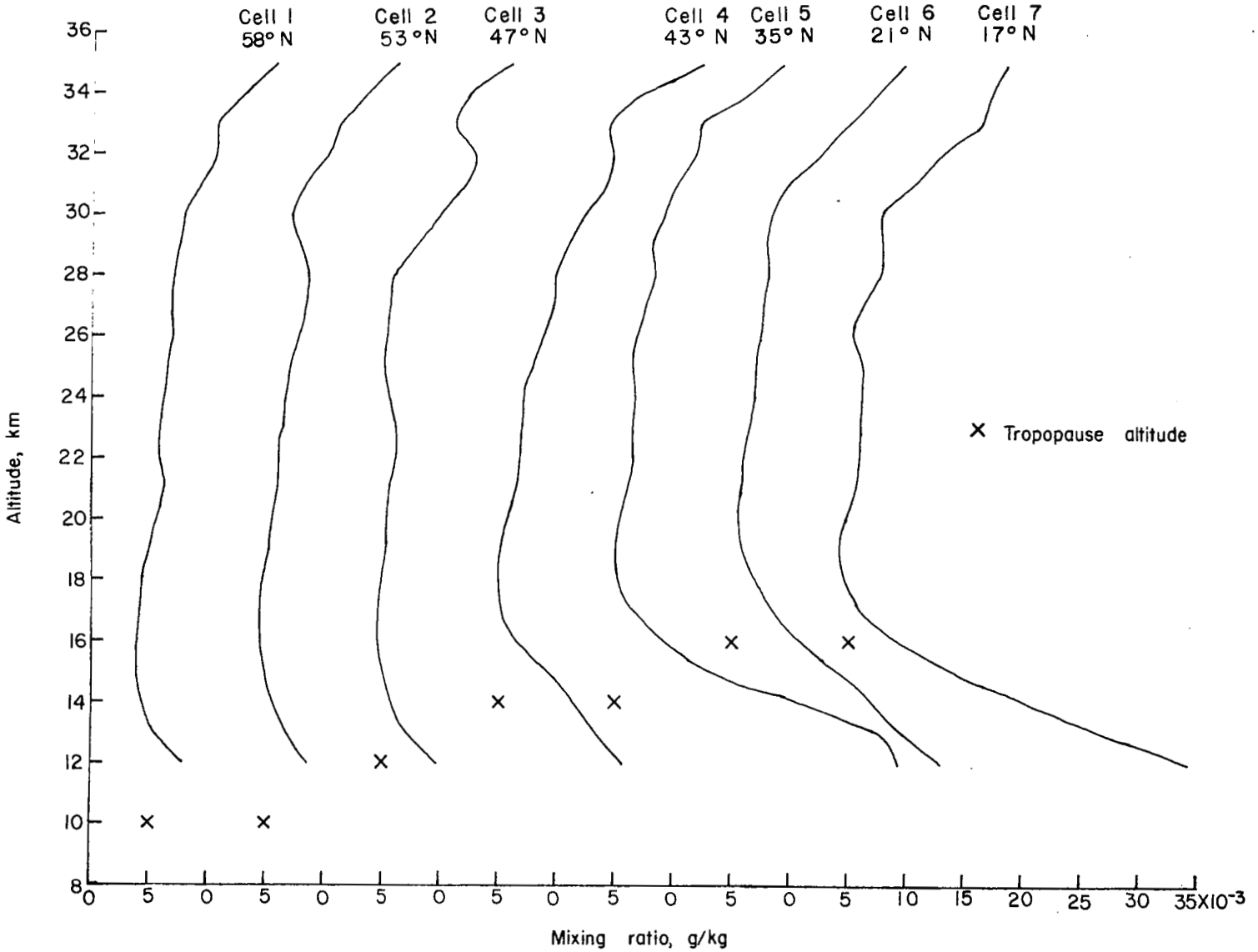

Figure 7.- Latitudinal variation of inferred mixing ratios from Project Scanner data obtained in August 1966. Data are plotted from table V.